Clays Clay Miner., Vol. 71, No. 4:416–429, 2023
https://doi.org/10.1007/s42860-023-00248-2

ORIGINAL PAPER

Silicon Incorporation Reduces the Reactivity of Short-range Ordered Aluminosilicates Toward Organic Acids

Katharina R. Lenhardt · Mathias Stein · Thilo Rennert

Accepted: 19 July 2023 / Published online: 11 August 2023

Abstract The structure and composition of short-range ordered aluminosilicates (SROAS) may control their affinity for organic acids with potential effects on soil organic matter stabilization. Adsorption mechanisms of model organic acids were studied to resolve the effect of Si incorporation. Adsorption of oxalic, salicylic, and octanoic acid on Al-rich (Al:Si = 3.7) and Si-rich (Al:Si = 1.4) SROAS was quantified by analyses of dissolved organic carbon using catalytic high-temperature combustion. The initial pH of 5 and 6.5 increased to 6.3–8.2 during adsorption of oxalic and salicylic acid, demonstrating hydroxyl release by ligand exchange. Minor changes in pH indicated weak interactions of octanoic acid with both SROAS. Adsorbates were characterized by Fourier-transform infrared spectroscopy. Asymmetric stretching of carboxylate groups at 1720 and 1700 cm^{-1}, and symmetric stretching at 1430 cm^{-1} evinced the formation of chelate complexes for oxalic acid. An absorption band centered at 1545 cm^{-1} indicated partial inner-sphere binding of salicylic acid on both SROAS. Silicon-rich SROAS adsorbed 80–90% less than Al-rich SROAS, suggesting that adsorption of oxalic and salicylic acid was controlled by surface aluminol groups. Fast kinetics of oxalate adsorption on Al sites was studied by a conductivity-based stopped-flow technique. Ligand exchange proceeded at a rate constant of 3.5 s^{-1} (25°C), similar to solute Al complexation, with an activation energy of up to 34.1 kJ mol^{-1}. A slow process with a rate constant of 0.13 s^{-1} (25°C) was attributed to diffusion of oxalate at the surface or into SROAS particles. As supported by structural characterization of Si-rich SROAS, the much lower susceptibility of Si-rich SROAS to ligand exchange relates to Al speciation. The formation of tetrahedral Al precludes its complexation by carboxyl groups.

Keywords Allophane · Fast adsorption kinetics · Imogolite · Ligand exchange · Soil organic matter

Associate Editor: William F. Jaynes

Supplementary Information The online version contains supplementary material available at https://doi.org/10.1007/s42860-023-00248-2.

K. R. Lenhardt (✉) · M. Stein · T. Rennert
Department of Soil Chemistry and Pedology, Institute of Soil Science and Land Evaluation, University of Hohenheim, Emil-Wolff-Str. 27, 70599 Stuttgart, Germany
e-mail: katharina.lenhardt@uni-hohenheim.de

M. Stein
e-mail: mathias.stein@zalf.de

T. Rennert
e-mail: t.rennert@uni-hohenheim.de

M. Stein
Working Group Silicon Biogeochemistry, Leibniz Centre for Agricultural Landscape Research (ZALF), 15374 Müncheberg, Germany

Introduction

Short-range ordered aluminosilicates (SROAS) are hydrous minerals that form frequently in the course of weathering of volcanic ejecta (Levard & Basile-Doelsch, 2016; Parfitt, 2009). At the nanoscale, these phases exhibit variable degrees of spatial order, including structurally defined tube-shaped imogolite (Cradwick et al., 1972). Moreover, primary particles may occur as hollow spheres and corresponding fragments with variable chemical composition, frequently referred to as allophane (Levard & Basile-Doelsch, 2016). Adsorption of dissolved organic matter (DOM) on SROAS is presumed to be a major pathway of soil organic matter (SOM) accrual because SROAS surfaces have a high affinity for DOM (Lilienfein et al., 2004; Singh et al., 2017). Carboxylic aromatic acids, derived from lignin degradation, are retained preferentially on SROAS (Ding et al., 2019; Lenhardt et al., 2022), forming stable bonds by displacing hydroxyls (OH^-) from the surface (Parfitt et al., 1977). Consequently, they are protected from microbial degradation, contributing to deceleration of SOM turnover in andic soils (Basile-Doelsch et al., 2005; Kramer et al., 2012; Torn et al., 1997).

Surface affinity of SROAS for carboxylic acids probably depends on chemical composition, which is governed by formation conditions. Aluminum-rich SROAS have molar Al:Si ratios of 2–4 and were detected in andic and podzolic soils (e.g. Gustafsson et al., 1999; Parfitt et al., 1980). In particular, Al-rich SROAS exhibit short-range order, namely, imogolite-like structural features (Cradwick et al., 1972; Goodman et al., 1985). A pronounced abundance of silicic acid facilitates Si incorporation into SROAS, and phases with Al:Si ratios of ~1 form. Such conditions may prevail in the early stages of tephra weathering (Gérard et al., 2007), when water availability restrains Si leaching (Parfitt et al., 1983), or during precipitation of stream deposits (Childs et al., 1990). Together with smaller Al contents, Si incorporation is accompanied by the formation of tetrahedral Al and condensation of Si tetrahedra, resulting in structural features similar to tectosilicates in Si-rich SROAS (Farmer et al., 1979; Ildefonse et al., 1994). Positive correlations of Al:Si ratios and amounts of adsorbed anions with high affinity for inner-sphere complexation (oxalate, fluoride, phosphate; Clarke & McBride, 1984; Hanudin et al., 2002; Kaufhold et al., 2010) suggest that Si incorporation diminishes SROAS reactivity toward carboxyl groups. This may be related to a lesser abundance of aluminol groups, as silanol groups do not participate in ligand exchange with organic functional groups (Pokrovski & Schott, 1998). On the other hand, silicic acid disturbs Al oxolation (Exley et al., 2002; Lenhardt et al., 2022), which may actually foster aluminol abundance. The formation of tetrahedral Al imparts negative charge on SROAS particles (Su et al., 1992). This may cause repulsion of oxidized DOM components, but facilitates hydrogen bonding or electrostatic interactions with amino groups. Sugars, nitrogenous compounds, and benzene derivatives adsorbed on SROAS by forces weaker than chemical binding (Hashizume & Theng, 2007; Nishikiori et al., 2009). Polymerized Si species provide variable charge to SROAS (Clarke & McBride, 1984; Su et al., 1992), and may thus contribute to electrostatic retention of organic substances. Hence, mechanistic studies are needed to resolve the effect of SROAS structure and composition on DOM binding.

Fourier-transform infrared (FTIR) spectroscopy was used to characterize the chemical environment of adsorbed functional groups on SROAS (e.g. Nishikiori et al., 2009; Parfitt et al., 1977). This technique allows for a differentiation of outer-sphere and inner-sphere complexes on Al-containing minerals (e.g. Axe & Persson, 2001; Parfitt et al., 1977). Evaluation of adsorption kinetics provides information on the rate-controlling processes and respective activation energies (Guan et al., 2006; Sparks, 1985) and is, thus, a tool to study the affinity of organic substances for SROAS surfaces in more detail. However, a suitable kinetic method must consider rapid reactions, because adsorption of organic molecules on Al-containing minerals equilibrates in the range of seconds to minutes (Borah et al., 2007; Das et al., 2004). This task may be accomplished by a conductivity-based stopped-flow technique that has been used frequently to study solute Al complexation and ion adsorption on minerals (e.g. Ikeda et al., 1984; Pohlmeier & Knoche, 1996).

The objective of the current study was to assess the impact of Si incorporation on SROAS surface reactivity toward different organic acids as models of natural DOM. For the first time, interaction mechanisms were elucidated by spectroscopic characterization of adsorbates together with the evaluation of

https://doi.org/10.1007/s42860-023-00248-2 Published online by Cambridge University Press

fast adsorption kinetics using structurally characterized SROAS. Synthesis of SROAS was performed at ambient conditions to mimic surface properties of natural, poorly ordered phases (Lenhardt et al., 2021). Oxalic, salicylic, and octanoic acid were used as models of functional moieties present in soil DOM. Oxalic and salicylic acid are introduced to soil solution by organic matter degradation and root exudation (Strobel, 2001). Oxalic acid, in particular, is able to displace OH^- from surface Al sites that may react with carboxyl groups in DOM (Hanudin et al., 2002; Parfitt et al., 1977). Salicylic acid contains phenolic groups presumably involved in binding of aromatic acids. Octanoic acid resembles hydrophobic aliphatic components from plant residues (Buurman et al., 2007). This study is based on the hypothesis that Si incorporation reduces the amount of surface sites susceptible to ligand exchange and, thus, the affinity of SROAS for organic acids.

Materials and Methods

Synthesis and characterization of SROAS

Two SROAS were synthesized at ambient conditions according to Lenhardt et al. (2021) by neutralizing Al-chloride hexahydrate ($AlCl_3$; AppliChem GmbH, Darmstadt, Germany) with sodium orthosilicate (Na_4SiO_4; abcr GmbH, Karlsruhe, Germany). The suspensions were dialyzed with a cellulose membrane (molecular weight cut-off 6–8 kD; Spectra Por 7, Repligen, Waltham, Massachusetts, USA) until the electrical conductivity of the permeate was <10 µS cm^{-1} for 24 h. Suspensions were subsequently stored at ambient temperature prior to use in batch experiments. The suspension concentration was determined gravimetrically after drying 5 mL of suspension at 105°C in triplicate. The element contents (Al, Si) of SROAS were determined by dissolving SROAS in 0.2 M HCl and subsequent quantification of Al and Si by microwave plasma-atomic emission spectrometry (MP-AES; 4200 MP-AES, Agilent, Waldbronn, Germany). The synthesized SROAS contained 199 and 262 mg Al g^{-1}, and 140 and 73 mg Si g^{-1}, resulting in molar Al:Si ratios of 1.4 and 3.7, respectively. Aliquots of suspensions were freeze-dried and ground in a mortar for mineral characterization by X-ray diffractometry (XRD) and FTIR spectroscopy. Samples were exposed to CoKα radiation (λ = 0.179 nm) and diffractograms recorded at a step size of 0.02°2θ and a counting time of 97.5 s with a Bruker D2 Phaser (Bruker, Ettlingen, Germany). Transmission FTIR spectra in the mid-infrared range were obtained with an external accessory of a LUMOS infrared microscope with a mercury-cadmium-telluride detector (Bruker) using pellets prepared with a hand press from a mixture of 1 mg of sample and 200 mg of KBr. Fifty background scans were recorded against the atmosphere and subsequently 100 sample scans accumulated at a resolution of 4 cm^{-1}. A Vertex 70 spectrometer equipped with a deuterated D-alanine-doped triglycine sulfate detector (Bruker) was used to obtain spectra in the far-infrared range at a resolution of 2 cm^{-1}. Pellets were prepared with a hydraulic press from a mixture of 1 mg of sample and 200 mg of KBr. Background scans were measured against the atmosphere before sample scans were recorded (64 scans each). The electrophoretic mobility of SROAS particles was measured in dilute suspensions (500 mg L^{-1}) at pH 5 and 6.5, and two concentrations of sodium chloride (NaCl, Chemsolute, Renningen, Germany; no addition of NaCl and 50 mmol L^{-1} NaCl). The electrophoretic mobility was analyzed by phase analysis light scattering using a Zetasizer Nano ZSP (Malvern Panalytical, Herrenberg, Germany) equipped with a helium-neon laser (λ = 633 nm) and a non-invasive backscatter detector at a fixed angle of 173°. Zeta potential was obtained by conversion of electrophoretic mobility data using the Smoluchowski approximation.

Batch-adsorption experiments

Adsorption of oxalic, salicylic, and octanoic acid was studied at initial pH 5 and 6.5, and 5 h contact time at room temperature. Batch experiments were performed in duplicate with a mass of 200 mg of adsorbent in 40 mL of background electrolyte solution (50 mmol L^{-1} NaCl) in 50 mL glass bottles with polytetrafluoroethylene caps. Total Al and Si concentrations in batch experiments were 995–1310 and 365–700 mg L^{-1}, respectively. Adsorption was quantified as a function of initial concentration (0–7.5 mmol L^{-1} for oxalic and salicylic acid, and 0–1.2 mmol L^{-1} for octanoic acid given its lower aqueous solubility). Stock solutions were prepared from oxalic acid dihydrate (25 mmol L^{-1}, AppliChem GmbH), sodium

https://doi.org/10.1007/s42860-023-00248-2 Published online by Cambridge University Press

salicylate (25 mmol L^{-1}, Merck KGaA, Darmstadt, Germany), and octanoic acid (3.5 mmol L^{-1}, Arcos Organics, Geel, Belgium). Stock solutions of octanoic acid were neutralized by dropwise addition of diluted NaOH (Chemsolute) to increase its solubility (Bell, 1973). The mass of SROAS, background electrolyte, and initial concentration of adsorptives were adjusted by mixing aliquots of stock solutions and SROAS suspensions previously adjusted to pH 5 or 6.5 with diluted HCl and NaOH (Chemsolute). Batches were shaken horizontally at 125 rpm, and phase separation was subsequently achieved by vacuum filtration with 0.22-µm polyether sulfone membranes (Merck Milipore, Burlington, Massachusetts, USA). The filtrates were analyzed for pH using a potentiometric electrode (Mettler Toledo, Gießen, Germany), and the concentrations of the remaining organic acids were quantified as dissolved organic carbon by catalytic high-temperature combustion using a DIMATOC 2100 (Dimatec, Essen, Germany). Filtrate Al and Si concentrations were quantified by MP-AES to detect possible SROAS dissolution.

Changes in pH during the first 30 min of contact between SROAS and adsorptives (c = 1.2 mmol L^{-1} each) were monitored at a resolution of 5 s in separate experiments (Seven Excellence S475, Mettler Toledo). Aliquots of stock solutions (NaCl, adsorptive) were pipetted into glass beakers, and the pH adjusted to 5 or 6.5. Detection of pH was initiated, and the SRAOS suspension (pH adjusted to 5 or 6.5) added after ~15 s under stirring to monitor rapid changes occurring as soon as SROAS were exposed to the adsorptives. The final volume was 20 mL. The mineral-to-solution ratio and the background electrolyte concentration equaled that in batches shaken for 5 h.

Adsorbed organic species were analyzed using air-dried filters from batches shaken for 5 h by diffuse reflectance infrared Fourier-transform (DRIFT) spectroscopy in the mid-infrared range again with the accessory of a LUMOS infrared microscope. Pestled samples (10 mg) were mixed with 150 mg of KBr. Fifty background scans were recorded from pure KBr, and 50 scans of each sample were accumulated. Spectra were normalized to the absorption maximum of Si–O–Al stretching vibrations (1020–970 cm^{-1}; Farmer et al., 1979). Difference spectra were calculated by subtracting spectra of pure SROAS (batch experiments with no organic acid added) from those of the adsorption variants. Reference DRIFT spectra of oxalic acid di-hydrate, sodium oxalate (Fluka Chemie AG, Buchs, Switzerland), salicylic acid (AppliChem GmbH), and sodium salicylate were obtained from mixtures of 3–10 mg of the compound with 100 mg of KBr.

Fast adsorption kinetics

Fast adsorption kinetics were investigated by monitoring the decline of electrical conductivity in SROAS suspensions immediately after addition of organic acids. Experiments were performed with a stopped-flow apparatus that allows for detection of conductivity changes <0.1% at a resolution of milliseconds (Hi-Tech CSF-21, TkG Scientific United, Wiltshire, United Kingdom). A dilute SROAS suspension and a solution containing an organic acid were stored in two parallel syringes and pressed simultaneously into a mixing cell. The cell had a volume of 21 µL, and mixing was complete after <30 ms. Electrical conductivity was traced ten times for 30 s at five temperatures (5, 10, 15, 20, 25°C) in individual experiments and averaged. Mineral suspensions had a mass concentration of 1 or 2 g L^{-1} and organic-acid concentration was 1 mmol L^{-1}, both were adjusted to pH 5. The background electrolyte was not adjusted to a specific concentration, but the electrical conductivity to the same level for suspension and adsorptive solution by dropwise addition of NaCl.

The approach yields information on reactions far from equilibrium, i.e. on forward reactions; backward reactions can be ignored (Sparks et al., 1996). Based on batch-adsorption experiments, reactant concentrations were adjusted to establish an excess of organic acid relative to surface sites to guarantee pseudo-first order conditions. Then, adsorption kinetics can be described by exponential functions to obtain rate constants of adsorption processes (Rennert et al., 2005; Sparks et al., 1996). Analysis of conductivity data indicated two relaxation effects with different rate constants (Supplementary Material, Fig. S1). Thus, the time(t)-dependent conductivity decay was fitted to a bi-exponential function:

$$\Delta K(t) = \Delta K_1 \exp\left(-k_1 t\right) + \Delta K_2 \exp\left(-k_2 t\right) + b \quad (1)$$

where $\Delta K(t)$ represents the cumulative time-dependent decay of conductivity, ΔK_1 and ΔK_2 the relative

https://doi.org/10.1007/s42860-023-00248-2 Published online by Cambridge University Press

contributions of the two processes, k_1 and k_2 the respective rate constants, and b the equilibrium conductivity of the system at a given temperature.

Evaluation of data obtained at different temperatures (5–25°C) yielded rate constants as a function of temperature. According to the Arrhenius equation, the temperature (T) dependency of rate constants is given by:

$$k = A \exp\left(-\frac{E_A}{RT}\right) \quad (2)$$

with the activation energy (E_A), the gas constant (R), and a pre-exponential factor (A). In logarithmic form ($\ln(k)$), k is a linear function of $1/T$ with the slope $-E_A/R$. The activation energies of the two processes were calculated from a linear fit of measured $\ln(k_i)$. Data analysis was performed using *OriginPro* 2020 (OriginLab, Northampton, Massachusetts, USA).

Results

Characterization of adsorbents

X-ray diffractograms of SROAS showed very broad reflections indicative of a poorly ordered structure and confirmed that no crystalline Al hydroxides had formed (Fig. S2). Stretching Si–O–Al vibrations caused a band centered at 1015 cm^{-1}, typical of Si-rich SROAS (Fig. S3a; Farmer et al., 1979). The band shifted to a lower wavenumber in Al-rich SROAS (970 cm^{-1}, Fig. S3b), as observed previously for natural proto-imogolites (Gustafsson et al., 1999; Parfitt et al., 1980). The presence of Si in imogolite-like configuration was confirmed by an absorption band close to 345 cm^{-1} (Fig. S4; Farmer et al., 1979). Infrared spectra of adsorbents were similar to those of SROAS previously characterized by ^{27}Al nuclear magnetic resonance (NMR) spectroscopy (Fig. S3; Lenhardt et al., 2021). High intensity of Al–OH bending vibrations close to 590 cm^{-1} evinced mainly octahedral coordination of Al in Al-rich SROAS. This band was less pronounced in spectra of Si-rich SROAS, and a shoulder related to OH bending centered at 690 cm^{-1} appeared, indicating tetrahedral Al and ill-defined Si species (Farmer et al., 1979; Lenhardt et al., 2021).

Zeta potentials confirmed differences in surface charge as expected from structural characterization. Irrespective of pH and NaCl concentration, the zeta potential of Al-rich SROAS exceeded that of Si-rich SROAS, indicating a more positive charge (Fig. S5). It decreased from 52.4 to 43.7 mV with increasing pH from 5 to 6.5 for Al-rich SROAS and more strongly for Si-rich SROAS, as it fell from 35.5 to –8.2 mV. Consistent with the greater Si content, this result confirmed the contribution of permanent negative charge by tetrahedral Al in Si-rich SROAS (Su et al., 1992).

Adsorption of organic acids

Release of Al and Si from SROAS during batch-adsorption experiments was negligible (Fig. S6). Aluminum-rich and Si-rich SROAS differed strongly in their affinity for oxalic and salicylic acid at both initial pH. However, the adsorbed amounts of both acids were similar for a given SROAS (Fig. 1). Dissolved organic acids were mostly in anionic form in the studied pH range, oxalic acid largely as oxalate (pK_{a1} = 1.25, pK_{a2} = 3.81 at 25°C), and the carboxyl group of salicylic acid was dissociated (pK_a (COOH) = 2.98 at 20°C). At initial pH 5, maximal adsorption of oxalic and salicylic acid on Al-rich SROAS reached 0.83–0.84 mmol g^{-1} and decreased to 0.51–0.63 mmol g^{-1} at initial pH 6.5. Maximal adsorption of both acids on Si-rich SROAS was reduced by 80–90%, relative to Al-rich SROAS. At initial pH 5, maximal adsorption of oxalic and salicylic acid on Si-rich SROAS was 0.09–0.17 mmol g^{-1} and decreased

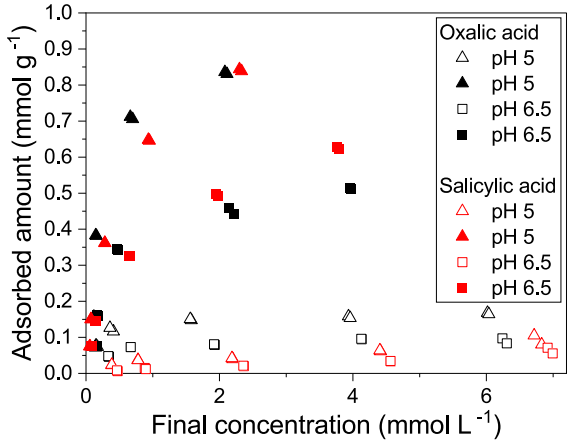

Fig. 1 Adsorption of oxalic acid and salicylic acid on short-range ordered aluminosilicates with molar Al:Si ratios of 1.4 (open symbols) and 3.7 (full symbols) at two initial pH values

https://doi.org/10.1007/s42860-023-00248-2 Published online by Cambridge University Press

Table 1 Maximum adsorption (*S*) of organic acids on two short-range ordered aluminosilicates normalized by Al content (*S* given in mmol g^{-1} Al^{-1}) as a function of initial pH, and molar adsorbate-to-Al ratios (Ratio). No octanoic acid was adsorbed at initial pH 6.5

Adsorbent (molar Al:Si ratio)		1.4		3.7	
initial pH		5	6.5	5	6.5
Adsorbate					
Oxalic acid ($C_2H_2O_4$)	*S*	0.84	0.45	3.17	1.95
	Ratio	0.023	0.012	0.086	0.053
Salicylic acid ($C_7H_6O_3$)	*S*	0.47	0.32	3.2	2.38
	Ratio	0.013	0.009	0.087	0.064
Octanoic acid ($C_8H_{16}O_2$)	*S*	0.52	–	0.47	–
	Ratio	0.014	–	0.013	–

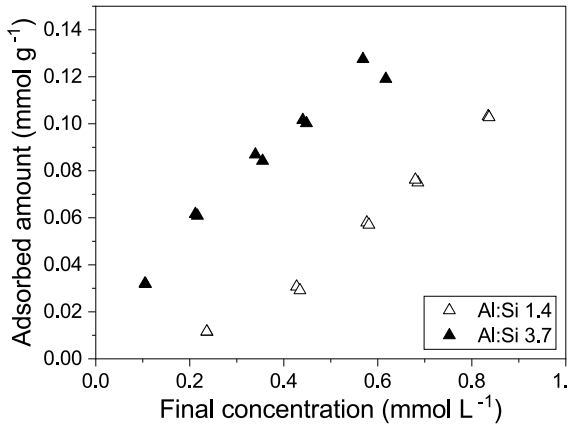

Fig. 2 Adsorption of octanoic acid on two short-range ordered aluminosilicates at initial pH 5

marginally to 0.06–0.09 mmol g^{-1} at initial pH 6.5. Because Al surface sites presumably control interactions with carboxylic acids (Parfitt et al., 1977), the amounts adsorbed were normalized to the adsorbents' Al contents (Table 1). The maximal amounts ranged from 1.95 to 3.17 mmol g^{-1} Al^{-1} for Al-rich SROAS and were 74–87% less for Si-rich SROAS (Table 1). Considering the marginal increase in adsorption on Si-rich SROAS at final concentrations >1.5 mmol L^{-1} (Fig. 1), measured maximal adsorption probably corresponded to the adsorption capacity of Si-rich SROAS.

The adsorption of oxalic and salicylic acid on SROAS raised the pH as a function of adsorbate quantity after 5 h (Fig. S7), indicating ligand exchange. According to time-dependent pH measurements, oxalic- and salicylic-acid adsorption equilibrated rapidly, as OH^- release occurred mostly within the first minute (Figs 3; S8). The increase in pH was greater for oxalic acid (0.8–1.9 units) evidencing more ligand exchange than for salicylic acid (0.3–0.9 units), as maximal adsorption of both oxalic and salicylic acid on a given SROAS was similar.

Adsorption of octanoic acid increased linearly with concentration at initial pH 5 for both Al- and Si-rich SROAS (Fig. 2). No adsorption was detected at initial pH 6.5. Octanoic acid has a greater pK_a (4.89 at 25°C) than oxalic and salicylic acid, indicating a greater proportion in undissociated form. Aluminum-rich and Si-rich SROAS differed only slightly in their affinity for octanoic acid. Maximal octanoic-acid adsorption was 0.12 mmol g^{-1} for Al-rich, and 0.1 mmol g^{-1} for Si-rich SROAS. Normalized to Al content, this also corresponded to similar amounts adsorbed (0.47–0.53 mmol g^{-1} Al^{-1}; Table 1). Due to solubility constraints, octanoic acid concentrations were probably not sufficient to reach adsorption capacity. No distinct OH^- release by octanoic-acid adsorption was observed within 30 min (Fig. 3).

Fast adsorption kinetics

Changes in electrical conductivity within 30 s were used to retrace adsorption reactions. Absolute changes in conductivity (ΔK) were poorly reproducible and <1 µS without addition of organic acids. Adsorption of octanoic and salicylic acid did not lead to greater ΔK values (≤0.6 and ≤1.1 µS, respectively). Although adsorption was most pronounced for oxalic acid on Al-rich SROAS at initial pH 5, ΔK at c(SROAS) = 0.5 g L^{-1} was 0.5–1.4 µS and did not increase with SROAS concentration (1 g L^{-1}; ΔK = 0.6–1.3 µS), indicating that conductivity was poorly related to decreasing oxalic-acid concentration. Adsorption of oxalic acid on Si-rich SROAS decreased conductivity by 1–1.7 µS at 0.5 g L^{-1} and 1.5–2.4 µS at 1 g L^{-1}.

Altogether, ΔK cohered with pH changes in time-dependent analyses (Fig. 3). The release of OH^- consumes H_3O^+ ions, which have a distinctly larger molar conductivity than the anions of the organic acids under study (Table S1). At low concentrations, the molar conductivity of ions is approximately equal to limiting molar conductivities, i.e. 404 S cm^2 mol^{-1}

https://doi.org/10.1007/s42860-023-00248-2 Published online by Cambridge University Press

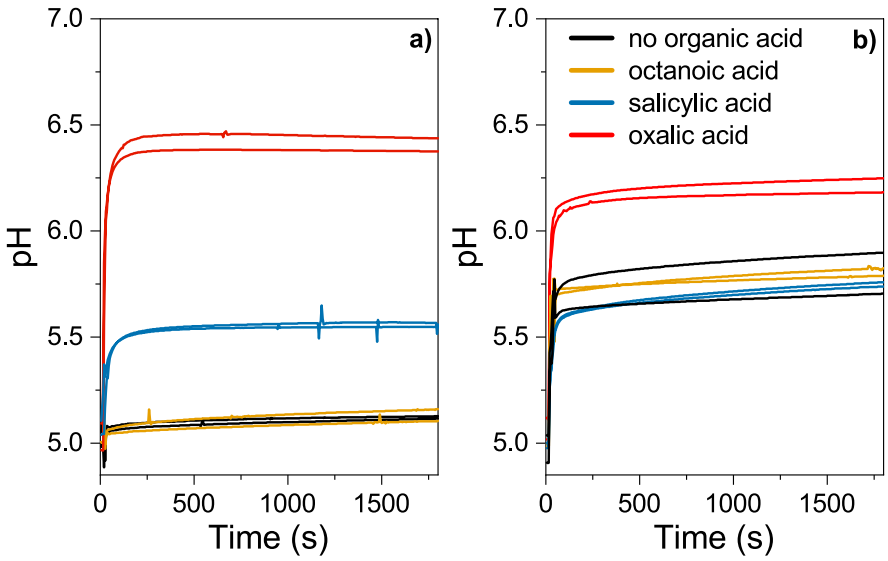

Fig. 3 Time-dependent pH change during adsorption of organic acids (1.2 mmol L^{-1}) on short-range ordered aluminosilicates with molar Al:Si ratios of **a** 1.4 and **b** 3.7 at initial pH 5

for H_3O^+ and 74.9 S cm^2 mol^{-1} for oxalate (Kinart, 2021). This implies that conductivity is particularly sensitive to ligand exchange. The effect of oxalic-acid adsorption on Al-rich SROAS on conductivity was small due to neutralization of OH^- in direct vicinity of the mineral surface, as supported by zeta potentials and time-dependent pH data. An increase in pH decreased the zeta potential only slightly, and the increase in pH was small relative to oxalic-acid adsorption (Fig. 3). Both indicate greater buffering by Al-rich SROAS. This is probably related to the greater affinity of aluminol groups for protons compared to silanol groups. Oxygen in aluminol groups is more polarized than oxygen in silanol groups, as the electronegativity differs between Al and Si (Essington, 2004).

Given the pronounced buffering of Al-rich SROAS, evaluation of the time-dependent decay in conductivity was limited to oxalic-acid adsorption on Si-rich SROAS. Two exponential terms were necessary to reconstruct conductivity decay (Figs 4, S1), indicating at least two processes. The pre-exponential factors ΔK_1 and ΔK_2 (Table 2) were similar, suggesting equal contributions of both processes to cumulative conductivity decay. The rate constants of the two processes (k_1, k_2) differed (Table 2). Rate constants of the fast process (k_1) increased with temperature from 1.4 to 3.5 s^{-1}, while those of the slow process (k_2) increased from 0.11 to 0.13 s^{-1} at c(SROAS) = 0.5 g L^{-1}. Neither rate constant responded to an increase in SROAS concentration, which confirms that pseudo-first order conditions were established (Sparks et al., 1996). Activation energies according to the Arrhenius equation (Eq. 2; inset in Fig. 4) were 5.5 and 9.5 kJ mol^{-1} for the slow process at SROAS concentrations of

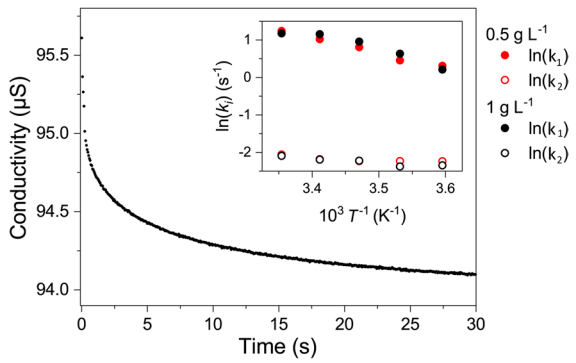

Fig. 4 Time-dependent conductivity decay due to adsorption of oxalic acid (0.5 mmol L^{-1}) on short-range ordered aluminosilicates (SROAS, Al:Si = 1.4; 1 g L^{-1}) at 25°C. The inset shows the Arrhenius plots for k_1 and k_2 at SROAS concentrations of 0.5 and 1 g L^{-1}

https://doi.org/10.1007/s42860-023-00248-2 Published online by Cambridge University Press

Table 2 Parameters obtained from fitting a bi-exponential function (Eq. 1) to conductivity decay observed in stopped-flow experiments. ΔK_1 and ΔK_2 represent relative changes in conductivity, k_1 and k_2 = rate constants, b = equilibrium conductivity, and R^2 is the coefficient of determination. Activation energies (E_A) were calculated from a linear fit of ln(k) using the Arrhenius equation (Eq. 2). R^2 and level of significance are given in parentheses

T (°C)	ΔK_1 (µS)	k_1 (s^{-1})	ΔK_2 (µS)	k_2 (s^{-1})	b (µS)	R^2
Al:Si 1.4 (0.5 g L^{-1}), oxalic acid (0.5 mmol L^{-1}; initial pH 5)						
5	0.76	1.4	0.76	0.11	35.5	0.998
10	0.69	1.6	0.64	0.11	38.8	0.997
15	0.57	2.2	0.40	0.11	42.6	0.996
20	0.56	2.8	0.37	0.11	46.3	0.996
25	0.41	3.5	0.57	0.13	50.0	0.996
E_A (kJ mol^{-1})		33.4 ± 2.2		5.5 ± 2.2		
		(R^2 = 0.98; p<0.05)		(R^2 = 0.58; p<0.1)		
Al:Si 1.4 (1 g L^{-1}), oxalic acid (0.5 mmol L^{-1}; initial pH 5)						
5	0.89	1.2	1.3	0.1	65.5	0.998
10	0.71	1.9	0.82	0.09	72.5	0.996
15	0.68	2.6	0.62	0.11	79.3	0.995
20	0.71	3.2	0.55	0.11	86.6	0.995
25	0.78	3.2	0.64	0.12	94.1	0.995
E_A (kJ mol^{-1})		34.1 ± 5.9		9.5 ± 2.1		
		(R^2 = 0.89; p<0.05)		(R^2 = 0.83; p<0.05)		

0.5 and 1 g L^{-1}, respectively (Table 2). Both the rate constants and the magnitude of activation energies are similar to a relaxation effect detected for fast adsorption of ferrocyanide on birnessite (Rennert et al., 2005). The slow process is presumably diffusion-controlled because of the low activation energy (Sparks, 1985). The activation energies of the fast process were greater and ranged from 33.4 to 34.1 kJ mol^{-1} (Table 2). Activation energies of partial inner-sphere complexation of small aromatic acids on aluminum (hydr)oxides were 31.3–47.9 kJ mol^{-1} (Das et al., 2004; Guan et al., 2006). Furthermore, the rate constant of the fast process was similar to rate constants (25°C) of ligand exchange between monomeric Al and chloroacetate (1.1 s^{-1}), fluoride (4 s^{-1}), and formate (10 s^{-1}; Pohlmeier et al., 1993). The fast process is, therefore, attributed to ligand exchange by oxalate with surface aluminol groups. Rates of proton dissociation or association are too fast to be detected in the applied approach (Pohlmeier & Knoche, 1996). Hence, the slow relaxation effect may be related to diffusive transport of oxalate at the surface ('film diffusion') or into SROAS particles ('intraparticle diffusion').

FTIR analyses of adsorbed organic acids

Adsorbed organic acids were analyzed by FTIR spectroscopy to verify adsorption modes. Generally, the intensity of vibrations from organic functional groups was proportional to the amount of organic acid adsorbed (Fig. 5). Absorption of functional groups of octanoic acid adsorbed on SROAS was too low for interpretation. Band positions and the relative intensities of oxalic and salicylic acid did not vary between Al- and Si-rich SROAS, pH, or organic-acid concentrations.

The high molecular symmetry of aqueous oxalate results in two defined absorption bands in infrared spectra caused by asymmetric and symmetric C–O stretching vibrations (1570 and 1280 cm^{-1}; Axe & Persson, 2001). Interactions with mineral surfaces modify the electronic structure of carboxylate groups, and cause band shifts and additional peaks. Marked absorption at 1720, 1700, 1430, and 1300 cm^{-1} in difference spectra of adsorbed oxalic acid (Fig. 5a) indicate the formation of bidentate inner-sphere complexes, as asymmetric stretching vibrations were shifted to higher wavenumbers (1720, 1700 cm^{-1}),

https://doi.org/10.1007/s42860-023-00248-2 Published online by Cambridge University Press

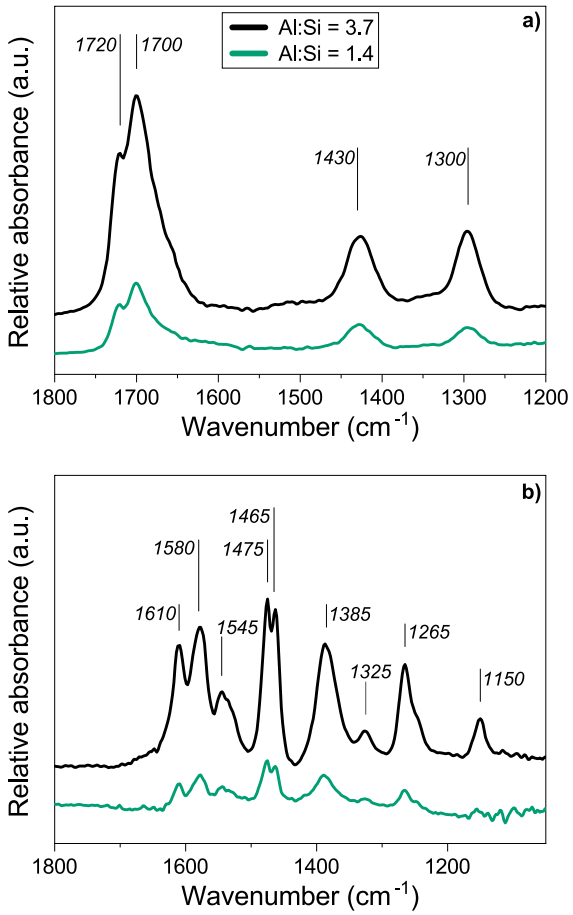

Fig. 5 Difference spectra of adsorption complexes formed by interaction of **a** oxalic and **b** salicylic acid with short-range ordered aluminosilicates at initial pH 5 obtained by diffuse reflectance infrared Fourier-transform spectroscopy. Absorbance is given in arbitrary units (a.u.) relative to absorption bands of Si–O–Al stretching vibrations (1020–970 cm^{-1}) in SROAS

and symmetric stretching of C–O bonds appeared at 1430 cm^{-1} (Axe & Persson, 2001). This is confirmed by reference spectra of oxalic acid di-hydrate and Na oxalate with marked absorption by asymmetric C–O stretching at smaller wavenumbers (1570–1680 cm^{-1}, Fig. S9). Oxalic acid weakly bound to SROAS surfaces would also cause absorption close to 1570 cm^{-1} (Axe & Persson, 2001; Rosenqvist et al., 2003; Yoon et al., 2004), which was lacking in the spectra obtained in the current study. A distinct split of asymmetric C–O stretching (>60 cm^{-1}; Axe & Persson, 2001) would indicate monodentate binding of oxalic acid, which, however, was not the case. Intensity distribution is very similar to spectra of dissolved oxalate-Al complexes (Fujita et al., 1962), which supports the formation of mononuclear chelates.

Interactions of salicylate with Al hydroxides, monomeric Al and Fe caused absorption close to 1530 cm^{-1}, resulting from a shift in asymmetric stretching of carboxylate C–O due to complexation (Biber & Stumm, 1994; Guan et al., 2007; Yost et al., 1990). Hence, the band centered at 1545 cm^{-1} in difference spectra of adsorbed salicylic acid (Fig. 5b) indicated partial inner-sphere complexation of carboxyl groups. This was confirmed by its absence from reference spectra of Na salicylate (Fig. S10). The band at 1580 cm^{-1} (Fig. 5b) was attributed to both aromatic C–C and asymmetric C–O carboxylate stretching (Yost et al., 1990). This band disappeared following salicylate adsorption on illite (Kubicki et al., 1997). Hence, two bands related to asymmetric C–O stretching, and broad symmetric C–O stretching vibrations at 1385 cm^{-1} (Yost et al., 1990), indicated several interaction modes between salicylic acid and SROAS. Stretching vibrations of phenolic C–OH were centered at 1265 cm^{-1} with a shoulder close to 1245 cm^{-1} (Fig. 5b). Their positions depended on dissociation and surface interactions (Biber & Stumm, 1994; Yost et al., 1990). Phenolic C–OH stretching shifted downward to 1241 cm^{-1} and upward to 1266–1259 cm^{-1} upon adsorption on goethite and aluminum oxides, respectively (Biber & Stumm, 1994; Das et al., 2004; Yost et al., 1990). Biber and Stumm (1994) explained these shifts with hydrogen bonds on aluminum oxide, but inner-sphere complexation on goethite, as protonation of phenolic groups also caused blue shifts. Accordingly, the intensity pattern in difference spectra of adsorbed salicylic acid (Fig. 5b) indicated interactions of phenolic groups with SROAS surfaces by electrostatic forces.

Discussion

Characterization of SROAS

Spectral features of synthesized SROAS supported their structural similarity to natural Al-rich and Si-rich phases. The synthesized SROAS may be perceived as polynuclear species that contain Si in imogolite-like configuration locally, Al-rich SROAS in particular; or have features of Si-rich

https://doi.org/10.1007/s42860-023-00248-2 Published online by Cambridge University Press

phases, because the extension of ordered sheets was very small (Lenhardt et al., 2021). The conditions of synthesis (concentrations, ambient temperature) hindered the assembly of proto-imogolite-like fragments to tube- or sphere-shaped particles (Lenhardt et al., 2021; Thill, 2016). Proto-imogolites with Al:Si ratios >2 may form in soil with enhanced Al availability as shown for Podzols (Gustafsson et al., 1999; Young et al., 1980). As evinced from the pattern of O–H bending vibrations, Al was mainly in octahedral coordination in Al-rich SROAS, while Si-rich SROAS had ~30% of Al in tetrahedral coordination (Lenhardt et al., 2021). Negative zeta potentials at pH 6.5, which indicate a lower point of zero charge, supported the presence of tetrahedral Al in Si-rich SROAS (Su et al., 1992). Tetrahedral Al in SROAS forms either by condensation of aluminate ($Al(OH)_4^-$) with silicic acid at neutral to alkaline pH (Wada & Wada, 1981), or during incorporation of Si into Al olation complexes (Beardmore et al., 2016; Doucet et al., 2001). Both pathways may apply, as precipitation was rapid (Lenhardt et al., 2021). The chemical environment of tetrahedral Al in Si-rich SROAS is similar to tectosilicates (Ildefonse et al., 1994), i.e. Al is connected to four Si tetrahedra by corner-sharing.

Mechanisms of organic-acid adsorption on SROAS

The three organic acids under study interacted with SROAS surfaces by different mechanisms. Oxalic acid formed inner-sphere complexes with both carboxyl groups involved, i.e. mononuclear chelates with surface Al sites. There was no evidence of molecules retained by electrostatic forces only, so that interactions of oxalic acid with silanol groups were negligible. Less OH^- per adsorbed organic molecule was released by salicylic acid than by oxalic acid. Infrared spectra indicated that carboxyl groups of salicylic acid participated only partially in ligand exchange, and phenolic groups interacted through electrostatic forces with SROAS surfaces, forming outer-sphere complexes. As the amounts of oxalic and salicylic acid adsorbed coincided for Al- and Si-rich SROAS at both initial pH, salicylate adsorption is also related to the abundance of aluminol groups, while weak interactions with Si sites seem to be insignificant. Outer-sphere complexation is probably caused by a lower affinity of salicylate for ligand exchange than oxalate. Consistently, adsorption enthalpies of dicarboxylic acids are more exothermic than those of salicylic acid (Benoit et al., 1993).

Weaker interactions than ligand exchange controlled adsorption of octanoic acid, as no OH^- was released by adsorption. Octanoic-acid adsorption was favored by a decrease in pH, indicating that dissociated carboxyl groups interacted electrostatically with positively charged surface sites. Concordantly, retention of fatty acids by Al and Fe oxides involved carboxyl groups while the hydrophobic end did not interact with the surface (Chernyshova et al., 2011; McBride, 1980).

Effect of SROAS structure on organic-acid adsorption

Quantitative adsorption data indicated that the effect of mineral structure on adsorption depended on the adsorption mechanism. Maximum adsorption of all organic acids on Si-rich SROAS was similar, while adsorption of oxalic and salicylic acid on Al-rich SROAS exceeded significantly that of octanoic acid. Thus, electrostatic adsorption on positively charged surface sites seems less affected by the composition of SROAS than inner-sphere complexation. Adsorption of octanoic acid on SROAS was greater than on Al oxide (0.06 mmol g^{-1}; Benoit et al., 1993), indicating more surface sites per mass for both poorly crystalline SROAS.

In contrast, the amounts of oxalic and salicylic acid adsorbed on Si-rich SROAS resembled those detected for crystalline Al (hydr)oxides (boehmite, 0.14 mmol oxalate g^{-1}; Axe & Persson, 2001; gibbsite, 0.22 mmol salicylate g^{-1}; Molis et al., 2000; Al oxide, 0.11 mmol salicylate g^{-1}; Ainsworth et al., 1998). However, adsorption was significantly greater on Al-rich SROAS, surpassing the amounts detected for natural SROAS with lower Al:Si ratios (1–1.5, 0.6–0.8 mmol oxalate g^{-1}; initial pH 6; Hanudin et al., 2002). Ligand exchange of oxalic and salicylic acid with aluminol sites confirms that octahedral Al surface sites control SROAS reactivity toward carboxylic acids. Outer-sphere complexation of oxalate with doubly coordinated hydroxyl groups as found for crystalline Al hydroxides (Axe & Persson, 2001) did not occur because of the low crystallinity of Al-rich SROAS. The lower reactivity of Si-rich SRAOS toward carboxylic acids is mainly caused by a larger abundance of tetrahedral Al, as the difference between SROAS

https://doi.org/10.1007/s42860-023-00248-2 Published online by Cambridge University Press

in maximal adsorption normalized to Al content was large (74–87%). Incorporation of Si adds unreactive functional groups coordinated to Si to the surface; however, Al speciation controls the extent of inner-sphere complexation with carboxyl groups.

Silicon-rich SROAS may form preferentially during weathering of alkaline tephra, when silicic acid and Al are highly available (Schaller et al., 2021). Then, a significant amount of Al may precipitate in tetrahedral coordination (Farmer et al., 1979) so that fewer sites are available for ligand exchange with DOM, and less SOM is protected against microbial degradation by chemical bonds with mineral surfaces (Mikutta et al., 2007).

Kinetics of organic-acid adsorption on SROAS

Adsorption of oxalic and salicylic acid on SROAS equilibrated within seconds to minutes, as derived from OH^- release and conductivity decay. Resolving the adsorption kinetics for <1 min allowed for a differentiation of rate-controlling processes of surface interactions. In experiments with oxalic acid and Si-rich SROAS, two relaxation effects with different rates indicated diffusive transport of oxalic acid and ligand exchange with surface Al sites. Pseudo-first order rate constants of the ligand-exchange reaction were similar to those of complexation of monomeric Al and organic anions (salicylate, benzoate, formate, acetate) determined by stopped-flow conductivity measurements at 25°C (0.17 to 30 s^{-1}; Pohlmeier et al., 1993; Secco & Venturini, 1975). The rate constants decreased with the ligand's acidity, which may be related to a greater affinity of organic anions for protons of coordinated water with increasing dissociation constant (Pohlmeier et al., 1993). Likewise, the chemical properties of organic acids may affect the rate of ligand exchange with Al surface sites of SROAS. However, rate constants of inner-sphere complexation by organic acids on SROAS surfaces seem to be similar to rate constants of solute Al complexation.

Outer-sphere complexation in solution is very rapid, and exchange of water or OH^- from the inner hydration shell of Al is the rate-limiting step (Eigen & Wilkins, 1965; Pohlmeier & Knoche, 1996). Ligand exchange of oxalic acid at SROAS surfaces was followed by a slower, diffusion-controlled process, indicating that the rate of mass transfer through the Stern layer or into the particles affect overall adsorption kinetics, as suggested for molybdate adsorption on goethite (Lang et al., 2000). Similarly, phosphate adsorption on natural SROAS proceeded by initially rapid ligand exchange and slower subsequent phosphate uptake (Parfitt, 1989) that may relate to reactions at imperfections or diffusion into pores (Strauss et al., 1997). Diffusion of adsorptives into interstices of crystallites, resulting in slow equilibration, is particularly applicable for poorly crystalline minerals.

Conclusion

Uptake of Si accompanied by formation of tetrahedral Al results in a decreased affinity of SROAS for carboxylic acids because fewer aluminol sites are available for ligand exchange. However, Si-rich SROAS have a greater capacity for adsorption by electrostatic interactions than crystalline Al hydroxides. Partial inner-sphere complexation of salicylic acid and oxalic acid on SROAS, as detected by FTIR spectroscopy, was confirmed by the fast kinetics of oxalic-acid adsorption on Si-rich SROAS. Slow diffusive transport of oxalate along the SROAS surface or into the particles may follow adsorption. The rate of OH^- exchange at the SROAS surface resembles that of Al complexation with organic ligands in solution. The diminished formation of chemical bonds between Si-rich SROAS and organic acids may affect SOM accrual and stabilization during initial soil formation in volcanic ejecta.

Acknowledgments Funding of this study was received from the Deutsche Forschungsgemeinschaft (RE 2251/9-1). The authors gratefully acknowledge help with mineral syntheses and adsorption experiments from Johannes Herre, the technical assistance of Annerose Böttcher with MP-AES measurements, and support from Detlev Frobel and Ludger Herrmann with XRD analyses. Far-infrared spectroscopy was conducted at the Institute of Applied Physics, University of Tübingen. Alexander Gerlach, Frank Schreiber, and Maximilian Senft are thanked for access to and support of the equipment.

Authors' contributions K.R.L. and T.R. designed this study. Experimental work was performed by K.R.L. and M.S. K.R.L. wrote the original manuscript with contributions by T.R. and M.S. in terms of content. All authors reviewed and edited the manuscript.

Funding Open Access funding enabled and organized by Projekt DEAL. Funding of this study was received from the Deutsche Forschungsgemeinschaft (RE 2251/9-1).

Data availability The datasets generated during the current study will be provided upon reasonable request.

Code availability (Not applicable)

Declarations

Competing interests The authors declare that they have no known competing financial interests or personal relationships that could have appeared to influence the work reported in this paper.

References

Ainsworth, C. C., Friedrich, D. M., Gassman, P. L., Wang, Z., & Joly, A. G. (1998). Characterization of salicylate-alumina surface complexes by polarized fluorescence spectroscopy. *Geochimica et Cosmochimica Acta, 62*, 595–612.

Axe, K., & Persson, P. (2001). Time-dependent surface speciation of oxalate at the water-boehmite (γ-AlOOH) interface: Implications for dissolution. *Geochimica et Cosmochimica Acta, 65*, 4481–4492.

Basile-Doelsch, I., Amundson, R., Stone, W. E. E., Masiello, C. A., Bottero, J. Y., Colin, F., et al. (2005). Mineralogical control of organic carbon dynamics in a volcanic ash soil on La Réunion. *European Journal of Soil Science, 56*, 689–703.

Beardmore, J., Lopez, X., Mujika, J. I., & Exley, C. (2016). What is the mechanism of formation of hydroxyaluminosilicates? *Scientific Reports, 6*, 30913.

Bell, G. H. (1973). Solubilities of normal aliphatic acids, alcohols and alkanes in water. *Chemistry and Physics of Lipids, 10*, 1–10.

Benoit, P., Hering, J. G., & Stumm, W. (1993). Comparative study of the adsorption of organic ligands on aluminum oxide by titration calorimetry. *Applied Geochemistry, 8*, 127–139.

Biber, M. V., & Stumm, W. (1994). An in-situ ATR-FTIR Study: The surface coordination of salicylic acid on aluminum and iron(III) oxides. *Environmental Science and Technology, 28*, 763–768.

Borah, J. M., Das, M. R., & Mahiuddin, S. (2007). Influence of anions on the adsorption kinetics of salicylate onto α-alumina in aqueous medium. *Journal of Colloid and Interface Science, 316*, 260–267.

Buurman, P., Peterse, F., & Almendros Martin, G. (2007). Soil organic chemistry in allophanic soils: A pyrolysis-GC/MS study of a Costa Rican Andosol catena. *European Journal of Soil Science, 58*, 1330–1347.

Chernyshova, I. V., Ponnurangam, S., & Somasundaran, P. (2011). Adsorption of fatty acids on iron (hydr)oxides from aqueous solutions. *Langmuir, 27*, 10007–10018.

Childs, C. W., Parfitt, R. L., & Newman, R. H. (1990). Structural studies of Silica Springs allophane. *Clay Minerals, 25*, 329–341.

Clarke, C. J., & McBride, M. B. (1984). Cation and anion retention by natural and synthetic allophane and imogolite. *Clays and Clay Minerals, 32*, 291–299.

Cradwick, P. D. G., Farmer, V. C., Russell, J. D., Masson, C. R., Wada, K., & Yoshinaga, N. (1972). Imogolite, a hydrated aluminum silicate of tubular structure. *Nature Physical Science, 240*, 187–189.

Das, M. R., Sahu, O. P., Borthakur, P. C., & Mahiuddin, S. (2004). Kinetics and adsorption behaviour of salicylate on α-alumina in aqueous medium. *Colloids and Surfaces A: Physicochemical and Engineering Aspects, 237*, 23–31.

Ding, Y., Lu, Y., Liao, P., Peng, S., Liang, Y., Lin, Z., et al. (2019). Molecular fractionation and sub-nanoscale distribution of dissolved organic matter on allophane. *Environmental Science: Nano, 6*, 2037–2048.

Doucet, F. J., Schneider, C., Bones, S. J., Kretchmer, A., Moss, I., Tekely, P., et al. (2001). The formation of hydroxyaluminosilicates of geochemical and biological significance. *Geochimica et Cosmochimica Acta, 65*, 2461–2467.

Eigen, M., & Wilkins, R. G. (1965). The kinetics and mechanism of formation of metal complexes. *Advances in Chemistry, 49*, 55–67.

Essington, M. E. (2004). *Soil and Water Chemistry: An Integrative Approach*. CRC Press.

Exley, C., Schneider, C., & Doucet, F. J. (2002). The reaction of aluminium with silicic acid in acidic solution: An important mechanism in controlling the biological availability of aluminium? *Coordination Chemistry Reviews, 228*, 127–135.

Farmer, V. C., Fraser, A. R., & Tait, J. M. (1979). Characterization of the chemical structures of natural and synthetic aluminosilicate gels and sols by infrared spectroscopy. *Geochimica et Cosmochimica Acta, 43*, 1417–1420.

Fujita, J., Martell, A. E., & Nakamoto, K. (1962). Infrared spectra of metal chelate compounds. VI. A normal coordinate treatment of oxalato metal complexes. *The Journal of Chemical Physics, 36*, 324–331.

Gérard, M., Caquineau, S., Pinheiro, J., & Stoops, G. (2007). Weathering and allophane neoformation in soils developed on volcanic ash in the Azores. *European Journal of Soil Science, 58*, 496–515.

https://doi.org/10.1007/s42860-023-00248-2 Published online by Cambridge University Press

Goodman, B. A., Russell, J. D., Montez, B., Oldfield, E., & Kirkpatrick, R. J. (1985). Structural studies of imogolite and allophanes by aluminum-27 and silicon-29 nuclear magnetic resonance spectroscopy. *Physics and Chemistry of Minerals, 12*, 342–346.

Guan, X.-H., Chen, G.-H., & Shang, C. (2006). Combining kinetic investigation with surface spectroscopic examination to study the role of aromatic carboxyl groups in NOM adsorption by aluminum hydroxide. *Journal of Colloid and Interface Science, 301*, 419–427.

Guan, X.-H., Chen, G.-H., & Shang, C. (2007). ATR-FTIR and XPS study on the structure of complexes formed upon the adsorption of simple organic acids on aluminum hydroxide. *Journal of Environmental Sciences, 19*, 438–443.

Gustafsson, J. P., Bhattacharya, P., & Karltun, E. (1999). Mineralogy of poorly crystalline aluminium phases in the B horizon of Podzols in southern Sweden. *Applied Geochemistry, 14*, 707–718.

Hanudin, E., Matsue, N., & Henmi, T. (2002). Reactions of some short-range ordered aluminosilicates with selected organic ligands. *Developments in Soil Science, 28*, 319–332.

Hashizume, H., & Theng, B. K. G. (2007). Adenine, adenosine, ribose and 5`-AMP adsorption to allophane. *Clays and Clay Minerals, 55*, 599–605.

Ikeda, T., Nakahara, J., Sasaki, M., & Yasunaga, T. (1984). Kinetic behavior of alkali metal ion on zeolite 4A surface using the stopped-flow method. *Journal of Colloid and Interface Science, 97*, 278–283.

Ildefonse, P., Kirkpatrick, R. J., Montez, B., Calas, G., Flank, A. M., & Lagarde, P. (1994). ^{27}Al MAS NMR and aluminum X-ray absorption near edge structure study of imogolite and allophanes. *Clays and Clay Minerals, 42*, 276–287.

Kaufhold, S., Dohrmann, R., Abidin, Z., Henmi, T., Matsue, N., Eichinger, L., et al. (2010). Allophane compared with other sorbent minerals for the removal of fluoride from water with particular focus on a mineable Ecuadorian allophane. *Applied Clay Science, 50*, 25–33.

Kinart, Z. (2021). Conductance studies of sodium salts of selected dicarboxylic acids in water at temperatures of 283.15 K to 313.15 K. *Journal of Molecular Liquids, 337*, 116262.

Kramer, M. G., Sanderman, J., Chadwick, O. A., Chorover, J., & Vitousek, P. M. (2012). Long-term carbon storage through retention of dissolved aromatic acids by reactive particles in soil. *Global Change Biology, 18*, 2594–2605.

Kubicki, J. D., Itoh, M. J., Schroeter, L. M., & Apitz, S. E. (1997). Bonding mechanisms of salicylic acid adsorbed onto illite clay: An ATR- FTIR and molecular orbital study. *Environmental Science and Technology, 31*, 1151–1156.

Lang, F., Pohlmeier, A., & Kaupenjohann, M. (2000). Mechanism of molybdenum sorption to iron oxides using pressure-jump relaxation. *Journal of Plant Nutrition and Soil Science, 163*, 571–575.

Lenhardt, K. R., Breitzke, H., Buntkowsky, G., Mikutta, C., & Rennert, T. (2022). Interactions of dissolved organic matter with short-range ordered aluminosilicates by adsorption and co-precipitation. *Geoderma, 423*, 115960.

Lenhardt, K. R., Breitzke, H., Buntkowsky, G., Reimhult, E., Willinger, M., & Rennert, T. (2021). Synthesis of short-range ordered aluminosilicates at ambient conditions. *Scientific Reports, 11*, 4207.

Levard, C., & Basile-Doelsch, I. (2016). Geology and mineralogy of imogolite-type materials. *Developments in Clay Science, 7*, 49–65.

Lilienfein, J., Qualls, R. G., Uselman, S. M., & Bridgham, S. D. (2004). Adsorption of dissolved organic carbon and nitrogen in soils of a weathering chronosequence. *Soil Science Society of America Journal, 68*, 292–305.

McBride, M. B. (1980). Adsorption of fatty acid spin probes on amorphous alumina. *Journal of Colloid and Interface Science, 76*, 393–398.

Mikutta, R., Mikutta, C., Kalbitz, K., Scheel, T., Kaiser, K., & Jahn, R. (2007). Biodegradation of forest floor organic matter bound to minerals via different binding mechanisms. *Geochimica et Cosmochimica Acta, 71*, 2569–2590.

Molis, E., Barrès, O., Marchand, H., Sauzéat, E., Humbert, B., & Thomas, F. (2000). Initial steps of ligand-promoted dissolution of gibbsite. *Colloids and Surfaces A: Physicochemical and Engineering Aspects, 163*, 283–292.

Nishikiori, H., Shindoh, J., Takahashi, N., Takagi, T., Tanaka, N., & Fujii, T. (2009). Adsorption of benzene derivatives on allophane. *Applied Clay Science, 43*, 160–163.

Parfitt, R. L. (1989). Phosphate reactions with natural allophane, ferrihydrite and goethite. *Journal of Soil Science, 40*, 359–369.

Parfitt, R. L. (2009). Allophane and imogolite: Role in soil biogeochemical processes. *Clay Minerals, 44*, 135–155.

Parfitt, R. L., Fraser, A. R., Russell, J. D., & Farmer, V. C. (1977). Adsorption on hydrous oxides II. Oxalate, benzoate and phosphate on gibbsite. *Journal of Soil Science, 28*, 40–47.

Parfitt, R. L., Furkert, R. J., & Henmi, T. (1980). Identification and structure of two types of allophane from volcanic ash soils and tephra. *Clays and Clay Minerals, 28*, 328–334.

Parfitt, R. L., Russell, M., & Orbell, G. E. (1983). Weathering sequence of soils from volcanic ash involving allophane and halloysite, New Zealand. *Geoderma, 29*, 41–57.

Pohlmeier, A., & Knoche, W. (1996). Kinetics of the complexation of Al^{3+} with aminoacids, IDA and NTA. *International Journal of Chemical Kinetics, 28*, 125–136.

Pohlmeier, A., Thesing, U., & Knoche, W. (1993). Formation of aluminium(III)-monocarboxylates in aqueous solution. *Berichte der Bunsengesellschaft für Physikalische Chemie, 97*, 10–15.

Pokrovski, G. S., & Schott, J. (1998). Experimental study of the complexation of silicon and germanium with aqueous organic species: Implications for germanium and silicon transport and Ge/Si ratio in natural waters. *Geochimica et Cosmochimica Acta, 62*, 3413–3428.

Rennert, T., Pohlmeier, A., & Mansfeldt, T. (2005). Oxidation of ferrocyanide by birnessite. *Environmental Science and Technology, 39*, 821–825.

Rosenqvist, J., Axe, K., Sjöberg, S., & Persson, P. (2003). Adsorption of dicarboxylates on nano-sized gibbsite particles: Effects of ligand structure on bonding mechanisms.

Colloids and Surfaces A: Physicochemical and Engineering Aspects, 220, 91–104.

Schaller, J., Puppe, D., Kaczorek, D., Ellerbrock, R., & Sommer, M. (2021). Silicon cycling in soils revisited. *Plants, 10*, 295.

Secco, F., & Venturini, M. (1975). Mechanism of complex formation. Reaction between aluminum and salicylate ions. *Inorganic Chemistry, 14*, 1978–1981.

Singh, M., Sarkar, B., Hussain, S., Ok, Y. S., Bolan, N. S., & Churchman, G. J. (2017). Influence of physico-chemical properties of soil clay fractions on the retention of dissolved organic carbon. *Environmental Geochemistry and Health, 39*, 1335–1350.

Sparks, D. L. (1985). Kinetics of ionic reactions in clay minerals and soils. *Advances in Agronomy, 38*, 231–265.

Sparks, D. L., Fendorf, S. E., Toner, C. V., & Carski, T. H. (1996). Kinetic methods and measurements. In D. L. Sparks (Ed.), *Methods of Soil Analysis, Part 3: Chemical Methods* (pp. 1275–1307). Soil Science Society of America Inc.

Strauss, R., Brümmer, G. W., & Barrow, N. J. (1997). Effects of crystallinity of goethite: II. Rates of sorption and desorption of phosphate. *European Journal of Soil Science, 48*, 101–114.

Strobel, B. W. (2001). Influence of vegetation on low-molecular-weight carboxylic acids in soil solution – a review. *Geoderma, 99*, 169–198.

Su, C., Harsh, J. B., & Bertsch, P. M. (1992). Sodium and chloride sorption by imogolite and allophanes. *Clays and Clay Minerals, 40*, 280–286.

Thill, A. (2016). From molecular precursor to imogolite nanotubes. *Developments in Clay Science, 7*, 429–457.

Torn, M. S., Trumbore, S. E., Chadwick, O. A., Vitousek, P. M., & Hendricks, D. M. (1997). Mineral control of soil organic carbon storage and turnover. *Nature, 389*, 170–173.

Wada, S.-I., & Wada, K. (1981). Reactions between aluminate ions and orthosilicic acid in dilute, alkaline to neutral solutions. *Soil Science, 132*, 267–273.

Yoon, T. H., Johnson, S. B., Musgrave, C. B., & Brown, G. E. (2004). Adsorption of organic matter at mineral/water interfaces: I. ATR-FTIR spectroscopic and quantum chemical study of oxalate adsorbed at boehmite/water and corundum/water interfaces. *Geochimica et Cosmochimica Acta, 48*, 4505–4518.

Yost, E. C., Tejedor-Tejedor, M. I., & Anderson, M. A. (1990). In situ CIR-FTIR characterization of salicylate complexes at the goethite/aqueous solution interface. *Environmental Science and Technology, 24*, 822–828.

Young, A. W., Campbell, A. S., & Walker, T. W. (1980). Allophane isolated from a podsol developed on a non-vitric parent material. *Nature, 284*, 46–48.